Results in Physics 54 (2023) 107082

Contents lists available at ScienceDirect

Results in Physics

journal homepage: www.elsevier.com/locate/rinp

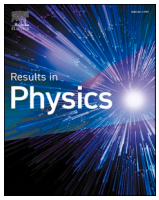

Magnetic properties of CoNi nanowires and nanotubes: Insights from micromagnetic simulations and composition-dependent equations

Diana M. Arciniegas Jaimes [a,b], Julieta M. Carballo [c], Martín I. Broens [a,d], Mariano Bruno [c], Felipe Tejo [e], Eduardo Saavedra [f], Juan Escrig [f,g,*], Noelia Bajales [d,h,*]

[a] Universidad Nacional de Córdoba (UNC), Facultad de Ciencias Químicas, 5000 Córdoba, Argentina
[b] CONICET, INFIQC, X5000HUA Córdoba, Argentina
[c] Universidad Nacional de Rio Cuarto (UNRC), Instituto de Investigaciones en Tecnologías Energéticas y Materiales Avanzados (IITEMA, CONICET, FCEFQyN), Rio Cuarto, Argentina
[d] CONICET, IFEG, 5000 Córdoba, Argentina
[e] Universidad Central de Chile, Escuela de Ingeniería, 8330601 Santiago, Chile
[f] Universidad de Santiago de Chile (USACH), Departamento de Física, 9170124 Santiago, Chile
[g] Center for the Development of Nanoscience and Nanotechnology (CEDENNA), 9170124 Santiago, Chile
[h] Universidad Nacional de Córdoba (UNC), FAMAF, 5000 Córdoba, Argentina

ARTICLE INFO

Keywords:
A. metals and alloys
A. nanostructured materials
C. anisotropy
C. magnetization
D. computer simulations

ABSTRACT

We conducted micromagnetic simulations of CoNi nanowires and nanotubes to study their magnetic properties as a function of their composition. We found that the hysteresis curves for isolated CoNi nanowires exhibit a square trend with an easy axis of magnetization along the nanowire axis. The coercivity and normalized remanence show a U-shaped behavior, with maximum values at Ni and Co and minimum values for the $Co_{40}Ni_{60}$ alloy. The hysteresis curves for CoNi nanotubes maintain the square trend of nanowires, but with a clear decrease in coercivity and an asymmetric V-shaped behavior for coercivity and normalized remanence. Our research offers valuable and comprehensive insights into the magnetic properties of CoNi nanowires and nanotubes. It underscores the significant influence of composition on magnetic properties, which holds great relevance for potential applications. Our approach, involving the prediction of static magnetic properties through micromagnetic simulations and tailored equations designed for nanostructures, rather than relying on bulk parameters, aligns more closely with the nature of these physical systems. This alignment is validated by the strong agreement with previously reported experimental results. Our work lays a solid foundation for the deliberate design of CoNi nanowires and nanotubes with specific magnetic properties tailored for articular applications. We anticipate that our study will facilitate the development of innovative magnetic nanostructures with controllable properties and enhanced performance.

Introduction

Magnetic nanowires (NWs) and nanotubes (NTs) have garnered considerable attention in recent years due to their diverse range of potential applications in fields such as biomedicine, environmental treatment, and spintronics [1–7]. These nanostructures, characterized by their elongated shape and high aspect ratio (length/diameter > 10) [8,9], often possess significant shape anisotropy. Moreover, the magnetic properties of NWs and NTs can be influenced by anisotropy, which is contingent upon both the composition and the synthesis process employed. Consequently, the resulting magnetic behavior of the nanostructures is governed by an effective anisotropy that arises from the interplay between shape anisotropy and the magnetocrystalline anisotropy within the system.

Nanostructures based on nickel (Ni) typically adopt a face-centered cubic (fcc) crystallographic phase, while cobalt-based (Co) nanostructures can exhibit either an fcc or a hexagonal close-packed (hcp) phase, depending on the synthesis conditions [10–19]. Consequently, CoNi alloys can manifest different crystallographic phases, providing the ability to tailor their magnetic properties [20,21]. This characteristic has led to the proposal of CoNi alloys for various potential applications [21–27].

* Corresponding authors.
E-mail addresses: juan.escrig@usach.cl (J. Escrig), noelia.bajales.luna@unc.edu.ar (N. Bajales).

https://doi.org/10.1016/j.rinp.2023.107082
Received 11 July 2023; Received in revised form 9 October 2023; Accepted 10 October 2023
Available online 17 October 2023

In this study, we conducted a comprehensive literature review to derive equations that accurately describe the magnetic properties of CoNi alloy across various cobalt percentages [2,13–20,28,29]. These equations represent a significant contribution to the scientific community, providing a theoretical framework for investigating the alloy using experimental parameters. Leveraging these equations, we performed micromagnetic simulations to investigate how the magnetic properties of CoNi nanowires and nanotubes change as a function of the percentage of cobalt in the alloy, i.e., the composition. We have focused our attention on the coercivity, remanence, and magnetization reversal mechanisms of these nanostructures as a function of their geometry (whether they are wires or tubes) and composition. By systematically varying the composition and geometry of the nanostructures, we aim to gain a deeper understanding of the underlying physics and provide insights for designing and optimizing CoNi-based magnetic nanostructures for various applications.

This paper is structured as follows: The second section presents the equations utilized to derive the magnetic parameters used in the simulations, along with a detailed description of the micromagnetic simulation methodology. In the third section, the results and discussion of this study are presented, while the final in the last section concludes the paper by summarizing the key findings and outlining prospects of our work.

Magnetic parameters

Due to the variability of magnetic parameters reported in the literature for Co_xNi_{100-x} alloy, which depends on the percentage of cobalt, we have compiled relevant data to derive general equations for these magnetic parameters, which will be attractive to both experimental and theoretical research groups. First, we digitized data for the stiffness constant, A, and saturation magnetization, M_S, using data obtained by Hinoul and Witters [30]. For the anisotropy constant, K_1, we used data obtained by Kadowaki and Takahashi [31], supplemented with measurements by Fan *et al.* [32], with the aim of obtaining more data for fitting the anisotropy constant. The resulting equations can be used to estimate magnetic parameters for various CoNi compositions.

After digitizing all the data for A, M_S, and K_1, we performed the corresponding fittings to obtain general equations for each magnetic parameter. The fittings made to the data obtained from previously published works [30–32] are shown in the supplementary information, see **Fig. S1**. The equations that describe the magnetic parameters of a Co_xNi_{100-x} alloy in the S.I units are as follows:

$$M_S(x) = 8674.26 \times x + 390425.99 \tag{1}$$

$$A(x) = e^{\left(-25.94-0.03\times x+\left(4.05\times 10^{-4}\right)\times x^2\right)} \tag{2}$$

$$K_1(x) = 23518.50 - 1013.28 \times x - 28486.22 \times e^{(-0.09\times x)} \tag{3}$$

Using the previous equations, we determined the magnetic parameters for different CoNi alloys, which are shown in Table 1.

Our statistical model's validity is confirmed by calculating the coefficient of determination (R^2), which yields values of 0.87, 0.97, and 0.98 for the adjustments of A, M_s, and K_1, respectively. This enables us to predict magnetic constants from the references we used with a high level of precision (for further details, see supplementary information, **Fig. S1**).

Table 1
Magnetic parameters obtained from Eqs. (1) to (3) for different compositions that will be investigated in this article.

Composition	M_S (A/m)	A (J/m)	K_1 (J/m^3)
Ni	390×10^3	0.53×10^{-11}	-4.97×10^3
$Co_{20}Ni_{80}$	564×10^3	0.33×10^{-11}	-1.46×10^3
$Co_{40}Ni_{60}$	737×10^3	0.27×10^{-11}	-17.80×10^3
$Co_{60}Ni_{40}$	910×10^3	0.32×10^{-11}	-37.40×10^3
$Co_{80}Ni_{20}$	1084×10^3	0.50×10^{-11}	-57.60×10^3
Co	1258×10^3	1.15×10^{-11}	-77.80×10^3

Micromagnetic simulations

The magnetic properties and magnetization reversal of CoNi NWs and NTs as a function of the composition were studied using micromagnetic simulations performed with the Object Oriented Micromagnetic Framework (OOMMF) software [33], which solves the Landau-Lifshitz-Gilbert equation (LLG) [34]. Our simulations are based on a continuum model that describes the magnetization dynamics of the nanostructures, considering the magnetic parameters defined in Table 1. At this point, it is important to note that we will consider a cubic magnetocrystalline anisotropy in our simulations [35–40].

In this study, we investigated the magnetic properties of CoNi cylindrical nanostructures with a length of 1000 nm, an external diameter of 100 nm, and for the nanotube case, a wall thickness of 30 nm [8]. A damping constant of $\alpha = 0.5$ was used for all simulations [41] for quick convergence, a standard practice in micromagnetic simulations without any significant deviations in the results. The simulation cell size of $2 \times 2 \times 10$ nm^3 was selected to balance accuracy and computational costs. This size was chosen to accommodate the extensive length of nanowires and nanotubes along the z-axis, while accurately replicating the cylindrical geometry of the nanostructures in the xy-plane. The hysteresis loops were obtained by applying a saturation field of 1000 mT with field steps of 2 mT in the z-direction.

Results and discussion

In this section, we show and discuss the results of our micromagnetic simulations for the magnetic properties of CoNi nanowires and nanotubes. We focus on the coercivity, remanence, and magnetization reversal mechanisms of these nanostructures as a function of their geometry and composition.

Variation of composition in CoNi nanowires

In Fig. 1**a**, we show hysteresis curves for isolated CoNi NWs of 1000 nm length and 100 nm diameter with different compositions, exhibited as a function of the percentage of cobalt present in the alloy. The complete simulated range for the applied magnetic field is depicted in the supplementary information (**Fig. S2**). In this illustration, the applied magnetic field spans from −40 to 40 mT, emphasizing the key features of the hysteresis loops. The hysteresis curves are quite square, indicating an easy axis of magnetization along the nanowire axis. From Fig. 1**b**, coercivity and normalized remanence exhibit a non-monotonic U-shaped behavior with maximum values at the extremes, Ni and Co, and minimum values for the $Co_{40}Ni_{60}$ alloy. Coercivity varies between approximately 0.010 T for $Co_{40}Ni_{60}$ and 0.030 T for Ni, while normalized remanence varies between 0.84 for $Co_{40}Ni_{60}$ and 0.94 for Ni, values very close to 1.0, which explains the square shape of the curves.

In order to explain the U-shaped behavior exhibited by the magnetic properties seen in Fig. 1**b**, it is important to remember that an increase in saturation magnetization, M_S, as observed in Table 1 with the increase in cobalt percentage, leads to a decrease in exchange length, $l_{ex} = \sqrt{2A/\mu_0 M_S^2}$, causing both coercivity and normalized remanence to decrease. This effect is enhanced by the decrease in the stiffness constant, A, observed between 0 and 80 % cobalt. The question then arises as to why do we see a resurgence in coercivity and remanence for percentages greater than 60 % cobalt? This increase in cobalt sample can be justified by the significant increase in stiffness constant. However, for the $Co_{60}Ni_{40}$ and $Co_{80}Ni_{20}$ alloys, the explanation lies in the magnetocrystalline anisotropy, K_1, which practically doubles the value obtained for $Co_{40}Ni_{60}$. Thus, we can observe that the magnetic behavior obtained

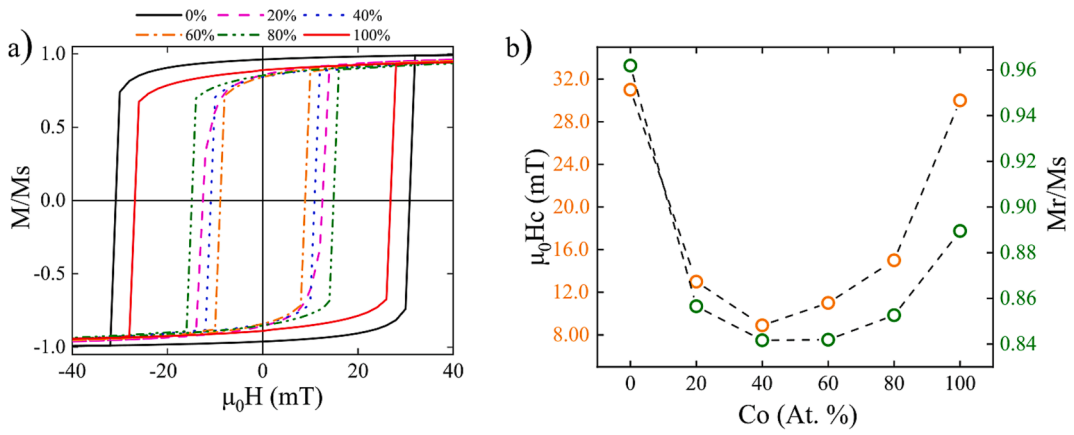

Fig. 1. (a) Hysteresis curves of isolated CoNi NWs with dimensions of 1000 nm length and 100 nm diameter, displaying variations in composition as a function of the percentage of cobalt in the alloy. The applied magnetic field ranges from −40 to 40 mT to emphasize key features in the loops. (b) Coercivity evolution (orange circles) and normalized remanence (green circles) for isolated CoNi NWs as a function of the percentage of cobalt in the alloy. (For interpretation of the references to colour in this figure legend, the reader is referred to the web version of this article.)

is a result of the competition between magnetostatic energy (M_S), exchange energy (A), and magnetocrystalline energy (K_1).

In order to further investigate how the magnetic parameters of the alloy affect the magnetic properties of the system, in Fig. 2 we have calculated the average values of the magnetic moment components as a function of position along the wire for different compositions. The idea is to be able to discriminate the mechanism by which the nanowires reverse their magnetization from point i to point f in the hysteresis curves. Since it is well-known that the reversal mode can change as a function of the geometric parameters of the system [32], our current focus is to investigate whether such changes could arise from variations of the magnetic parameters. For the Ni and $Co_{20}Ni_{80}$ cases, we can see that the average components of the magnetization, $<m_x>$ and $<m_y>$, are zero, which is a clear indicator that the nanostructure reverses its magnetization through the nucleation and propagation of vortex domain walls, something that had already been reported in the literature for large diameters [42,43]. However, for the $Co_{80}Ni_{20}$ and Co nanowires, we can see that the aforementioned components are not completely zero, so we can say that the nanowires reverse their magnetization through the nucleation and propagation of helical vortices. This change is due to the significant increase exhibited by both the stiffness constant, A, and the magnetocrystalline anisotropy constant, K_1. Experimental evidence of exotic transverse-vortex magnetic configurations in $Co_{85}Ni_{15}$ nanowires was recently reported by Andersen et al. [2]. These authors discovered that the magnetic configuration of CoNi nanowires is complex and inhomogeneous, with predominantly axial domains observed in the regions with a higher fcc composition. Their micromagnetic simulations demonstrated that a curling state, with a magnetic induction component oriented along the nanowire axis, appears in regions with fcc phase grains, where the easy axis and shape anisotropy act in the same manner. This study also highlights the strong correlation between crystal structure, composition, and the resulting magnetic configurations in CoNi nanowires, supporting the results we have presented here for a wide range of CoNi NW compositions. We have employed optimized magnetic parameters for nanoscale magnetic materials.

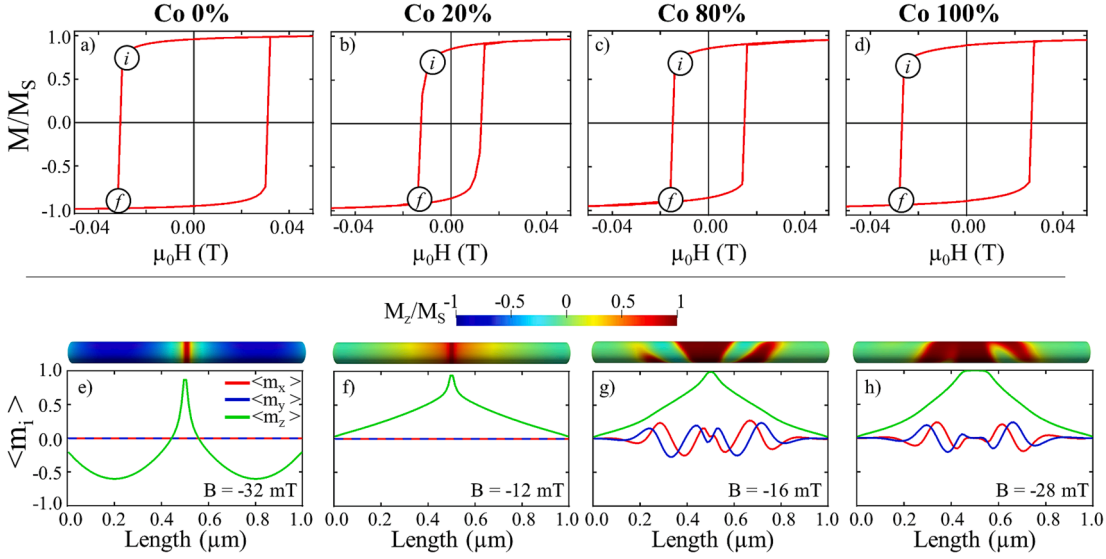

Fig. 2. Top panel: Hysteresis curves for CoNi NWs considering different compositions. The highlighted points i and f correspond to the investigated reversal process in the bottom panel. Bottom panel: Snapshots of magnetization reversal mechanisms for CoNi nanowires considering different compositions. The abscissa represents the length along the nanowire, while the ordinates account for the average magnetization components. $<m_x>$: solid red line; $<m_y>$: solid blue line, and $<m_z>$: solid green line. (For interpretation of the references to colour in this figure legend, the reader is referred to the web version of this article.)

Variation of composition in CoNi nanotubes

In Fig. 3**a**, we show the hysteresis curves for isolated CoNi NTs with a length of 1000 nm, outer diameter of 100 nm, and a wall thickness of 30 nm, considering different compositions presented as a function of the percentage of cobalt present in the alloy. The complete simulated range for the applied magnetic field is depicted in the supplementary information (**Fig. S2**). In this illustration, the applied magnetic field spans from −40 to 40 mT, emphasizing the key features of the hysteresis loops. Although the hysteresis curves maintain the square trend of the wires, a clear decrease in coercivity is observed. From Fig. 3**b**, we can see that both coercivity and normalized remanence show an asymmetric V-shaped behavior, different from the behavior observed for the case of nanowires, which exhibited a fairly symmetric U-shaped behavior. In this case, the minimum value for coercivity and normalized remanence is obtained for a $Co_{20}Ni_{80}$ alloy, i.e., the minimum moves towards an alloy with a lower percentage of cobalt when working with NTs. In this case, coercivity varies between approximately 0.005 T for $Co_{20}Ni_{80}$ and 0.020 T for Co (values that are almost half of those obtained for nanowires), while normalized remanence varies between 0.83 for $Co_{20}Ni_{80}$ and 0.94 for Ni, values very close to those obtained for nanowires. It is important to note that the maximum coercivity of the wires is obtained for a nickel nanowire, while the maximum coercivity of the tubes is obtained for a cobalt nanotube. A close comparison of our results obtained from micromagnetic simulations with those reported in experimental data by various authors reveals excellent agreement. For instance, Parajuli et al. [17] found a coercivity of approximately 750 Oe for $Co_{50}Ni_{50}$ NTs with a diameter of 100 nm fabricated by DC electrodeposition, while we have obtained a value of 7.5 mT for the same composition and diameter in CoNi NTs using the magnetic parameters proposed herein.

Next, in Fig. 4, we have calculated the average values of the magnetic moment components as a function of position along the NTs for different compositions. As with the NWs, the idea is to be able to discriminate the mechanism by which the NTs reverse their magnetization from point *i* to point *f* in the hysteresis curves. Similar to what was observed for the NWs, for both Ni and $Co_{20}Ni_{80}$ cases, we can see that the average magnetization components, $\langle m_x \rangle$ and $\langle m_y \rangle$, are zero, which is a clear indicator that the nanostructure reverses its magnetization through the nucleation and propagation of vortex domain walls. It is also reproduced that for $Co_{80}Ni_{20}$ NTs, the aforementioned components are different from zero, indicating that these nanotubes also reverse their magnetization through the nucleation and propagation of helical vortices. The significant difference occurs for the cobalt NT, where the system reverses its magnetization through vortex walls, unlike the case of the cobalt NW, which reversed its magnetization through helical vortices. This difference is because not only magnetic parameters define the magnetic properties of a system, but also its geometric parameters. Unlike some experimental studies, our approach in this study involves the consideration of a single, isolated structure to eliminate the influence of magnetostatic interactions with neighboring structures. Additionally, numerical modeling enables us to precisely align the direction of the applied magnetic field with the nanowire/nanotube axis.

Conclusions

Our micromagnetic simulations show that the composition and geometry of CoNi nanowires and nanotubes have a significant impact on their magnetic properties. Nanowires have a square hysteresis curve, indicating an easy axis of magnetization along the nanowire axis. The coercivity and normalized remanence exhibit a U-shaped behavior with maximum values at the extremes, Ni and Co, and minimum values for the $Co_{40}Ni_{60}$ alloy. The magnetic behavior obtained is a result of the competition between magnetostatic energy, exchange energy, and magnetocrystalline energy. The nanowires reverse their magnetization through the nucleation and propagation of vortex or helical vortices, depending on their composition. On the other hand, the hysteresis curves for isolated CoNi nanotubes also maintain the square trend of the nanowires, but with a clear decrease in coercivity. The coercivity and normalized remanence show an asymmetric V-shaped behavior, with the minimum value for both obtained for a $Co_{20}Ni_{80}$ alloy. The maximum coercivity of the nanowires is obtained for a nickel nanowire, while the maximum coercivity of the tubes is obtained for a cobalt nanotube. These results highlight the importance of careful design and optimization of CoNi nanostructures for specific applications.

CRediT authorship contribution statement

Diana M. Arciniegas Jaimes: Data curation, Investigation, Methodology, Writing – original draft, Writing – review & editing. **Julieta M. Carballo:** Data curation, Investigation, Methodology, Writing – review & editing. **Martín I. Broens:** Data curation, Investigation, Writing – review & editing. **Mariano Bruno:** Data curation, Investigation. **Felipe Tejo:** Data curation, Investigation, Methodology, Resources, Writing – review & editing. **Eduardo Saavedra:** Data curation, Investigation, Methodology, Resources, Writing – review & editing. **Juan Escrig:** . **Noelia Bajales:** .

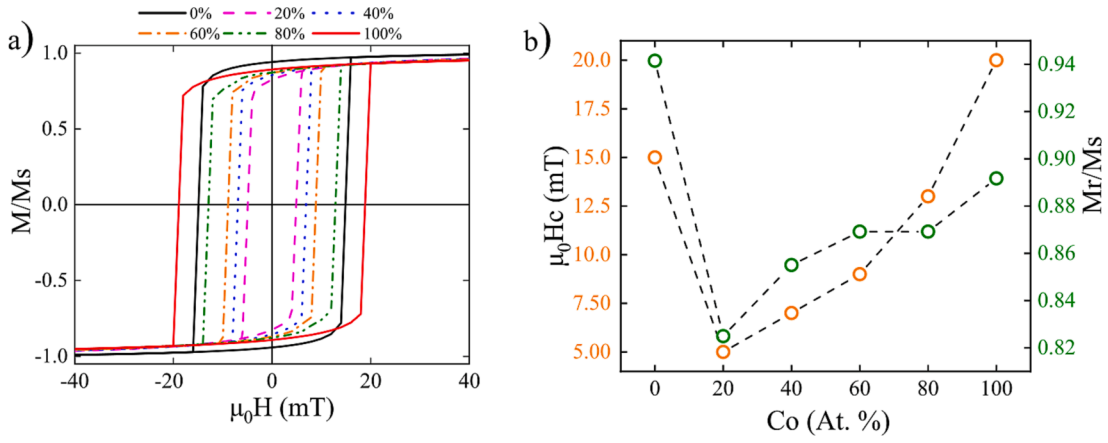

Fig. 3. (a) Hysteresis curves of isolated CoNi NTs with dimensions of 1000 nm length and 100 nm diameter, displaying variations in composition as a function of the percentage of cobalt in the alloy. The applied magnetic field ranges from −40 to 40 mT to emphasize key features in the loops. (b) Coercivity evolution (orange circles) and normalized remanence (green circles) for isolated CoNi NTs as a function of the percentage of cobalt present in the alloy. (For interpretation of the references to colour in this figure legend, the reader is referred to the web version of this article.)

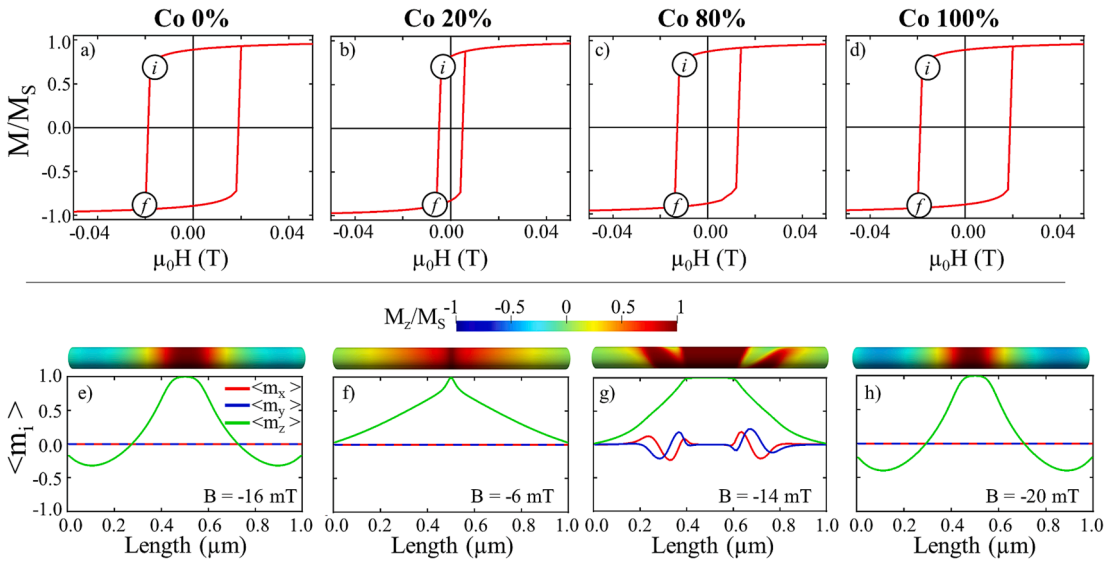

Fig. 4. Top panel: Hysteresis curves for CoNi NTs considering different compositions. The highlighted points *i* and *f* correspond to the investigated reversal process in the bottom panel. Bottom panel: Snapshots of magnetization reversal mechanisms for CoNi NTs considering different compositions. The abscissa represents the length along the nanotube, while the ordinates account for the average magnetization components. $<m_x>$: solid red line; $<m_y>$: solid blue line, and $<m_z>$: solid green line. (For interpretation of the references to colour in this figure legend, the reader is referred to the web version of this article.)

Declaration of Competing Interest

The authors declare that they have no known competing financial interests or personal relationships that could have appeared to influence the work reported in this paper.

Data availability

Data Availability The datasets generated during and/or analysed during the current study are available from the corresponding author on reasonable request.

Acknowledgements

The authors acknowledge financial support by Fondecyt 1200302, Dicyt-USACH 042331SD and Financiamiento Basal para Centros Científicos y Tecnológicos AFB220001, and CCAD-UNC for the cluster facilities. The work of F.T. was supported by ANID + Fondecyt de Postdoctorado, convocatoria 2022 + Folio 3220527. This research was partially supported by the supercomputing infrastructure of the NLHPC (ECM-02). D.M.A.J., M.I.B. and J.M.C. acknowledge CONICET for their fellowships.

Appendix A. Supplementary data

Supplementary data to this article can be found online at https://doi.org/10.1016/j.rinp.2023.107082.

References

[1] Proenca MP. Multifunctional Magnetic Nanowires and Nanotubes. *Multifunctional Magnetic Nanowires and Nanotubes* **Nanomaterials** 2022;12(8):1308.
[2] Andersen IM, Rodríguez LA, Bran C, Marcelot C, Joulie S, Hungria T, et al. Exotic Transverse-Vortex Magnetic Configurations in CoNi Nanowires. ACS Nano 2020;14 (2):1399–405.
[3] Aguilera-Granja F, Montejano-Carrizales J, Vogel E. Structural and oxidation properties of CoNi nanowires. Eur. Phys. J. D 2016;70:137.
[4] Almasi Kashi M, Ramazani A, Akhshi N, Khamse EJ, Fallah Z. The effect of pulsed electrodeposition parameters on the microstructure and magnetic properties of the CoNi nanowires. J Nanostr 2012;1:249–55.
[5] Andersen IM, Rodriguez LA, Wolf D, Lubk A, Bran C, Gatel C, et al. 2D and 3D Electron Holography Revealing Complex Magnetic Configurations in CoNi Nanowires. Microsc. Microanal. 2020;26(S2):1544–5.
[6] Pasquale M, Trabada DG, Olivetti ES, Sasso CP, Coisson M, Magni A, et al. Micromagnetic simulation of electrochemically deposited Co nanowire arrays for wideband microwave applications. **J. Phys. D Appl. Phys. in Press** 2023;56(48): 485001.
[7] Pathak S, Singh S, Gaur R, Sharma M. Experimental studies and micromagnetic simulations of electrodeposited Co nanotube arrays. J. Appl. Phys. 2014;116: 053904.
[8] Raviolo S, Arciniegas Jaimes DM, Bajales N, Escrig J. Wave reversal mode: A new magnetization reversal mechanism in magnetic nanotubes. J. Magn. Magn. Mater. 2020;497:165944.
[9] Raviolo S, Pereira A, Arciniegas Jaimes DM, Escrig J, Bajales N. Angular dependence of the magnetic properties of Permalloy nanowire arrays: A comparative analysis between experiment and simulation. J. Magn. Magn. Mater. 2020;499:166240.
[10] Pirota KR, Vázquez M. Arrays of electroplated multilayered Co/Cu nanowires with controlled magnetic anisotropy. Adv. Eng. Mater. 2005;7:1111.
[11] Vivas LG, Escrig J, Trabada DG, Badini-Confalonieri GA, Vázquez M. Magnetic anisotropy in ordered textured Co nanowires. Appl. Phys. Lett. 2012;100:252405.
[12] Vázquez M, Vivas LG. Magnetization reversal in Co-base nanowire arrays. Phys. Status Solidi B 2011;248(10):2368–81.
[13] Vivas LG, Vázquez M, Escrig J, Allende S, Altbir D, Leitao DC, et al. Magnetic anisotropy in CoNi nanowire arrays: Analytical calculations and experiments. Phys. Rev. B 2012;85:035439.
[14] Pereira A, Gallardo C, Espejo AP, Briones J, Vivas LG, Vázquez M, et al. Tailoring the magnetic properties of ordered 50-nm-diameter CoNi nanowire arrays. J. Nanopart. Res. 2013;15:2041.
[15] Zhang HM, Zhang XL, Zhang JJ, Li ZY, Sun HY. Fabrication and magnetic properties of CoNi alloy nanotube arrays. J. Magn. Magn. Mater. 2013;342:69.
[16] Pereira A, Palma JL, Vázquez M, Denardin JC, Escrig J. A soft/hard magnetic nanostructure based on multisegmented CoNi nanowires. PCCP 2015;17:5033.
[17] Parajuli S, Irfan M, Zhang XM, Javed K, Feng JF, Han XF. Diameter dependent structural and magnetic properties of CoNi alloy nanotubes. J. Magn. Magn. Mater. 2020;500:166264.
[18] Elkins J, Mohapatra J, Xing M, Beatty J, Liu JP. Structural, morphological and magnetic properties of compositionally modulated CoNi nanowires. J. Alloy. Compd. 2021;864:158123.
[19] Schöbitz M, Novotný O, Trapp B, Bochmann S, Cagnon L, Thirion C, et al. A material view on extrinsic magnetic domain wall pinning in cylindrical CoNi nanowires. J. Phys. Chem. C 2023;127(5):2387–97.
[20] Bran C, Fernandez-Roldan JA, del Real RP, Asenjo A, Chubykalo-Fesenko O, Vazquez M. Magnetic configurations in modulated cylindrical nanowires. Nanomat 2021;11:600.
[21] Andersen IM, Wolf D, Rodriguez LA, Lubk A, Oliveros D, Bran C, et al. Field tunable three-dimensional magnetic nanotextures in cobalt-nickel nanowires. Phys Rev Res 2021;3:033085.
[22] Vazquez M. Cylindrical nanowire arrays: From advanced fabrication to static and microwave magnetic properties. J. Magn. Magn. Mater. 2022;543:168634.
[23] Aslam MA, Ahsen R, Uddin W, ur Rehman S, Khan MS, Bilal M, et al. Tailoring the morphology of CoNi alloy by static magnetic field for electromagnetic wave absorption. The Europ Phys J plus 2022;137(4).
[24] Özdemir R, Korkmaz CA. Investigation of Structural and Magnetic Properties of Co. Ni and CoNi Alloy Thin Films by Fabricated with Electrodeposition, **El-Cezeri** 2022;9:1122–35.

[25] Rafique M, Yasir M, Pan L, Khan WS, Iqbal MZ, Qiu H, et al. Controlled synthesis, phase formation, growth mechanism, and magnetic properties of 3-D CoNi alloy microstructures composed of nanorods. Cryst Eng Comm 2013;15:5314–25.
[26] Bran C, Fernandez-Roldan JA, P. Del Real R, Asenjo A, Chen Y-S, Zhang J, et al. Unveiling the origin of multidomain structures in compositionally modulated cylindrical magnetic nanowires. ACS Nano 2020;14(10):12819–27.
[27] Xu Q, Wang Z-J, Wang Y-G, Sun H-Y. The effect of Co content on the structure and the magnetic properties of CoxNi1-x nanotubes. J. Magn. Magn. Mater. 2016;419:166–70.
[28] Chen N, Jiang J-T, Xu C-Y, Yan S-J, Zhen L. Rational Construction of Uniform CoNi-Based Core-Shell Microspheres with Tunable Electromagnetic Wave Absorption Properties. Sci. Rep. 2018;8:3196.
[29] Chen Y, Maaz K, Lyu S, Cheng Y, Liu J. Fabrication and temperature dependent magnetic properties of Co-Ni nanotube arrays. Physica e: Low-Dimensional Syst and Nanostr 2019;110:123–6.
[30] Hinoul M, Witters J. Exchange constants in nickel-cobalt alloys from standing spin wave resonance. Solid State Commun. 1972;10(9):749–52.
[31] Kadowaki S, Takahashi M. Magnetocrystalline anisotropy of nickel-cobalt alloys. J. Phys. Soc. Jpn. 1975;38:1612.
[32] Fan W-J, Ma Li, Shi Z, Zhou S-M. Fabrication and magnetocrystalline anisotropy of NiCo(002) films. Chinese Phys B 2015;24(3).
[33] Donahue MJ, Porter DG. OOMMF User's Guide. Version 2002;1.2a3. https://math.nist.gov/oommf.
[34] Mahalingam SS, Manikandan BV, Arockiaraj S. Review – micromagnetic simulation using OOMMF and experimental investigations on nano composite magnets. J. Phys. Conf. Ser. 2019;1172:012070.
[35] Adeela N, Maaz K, Khan U, Karim S, Ahmad M, Iqbal M, et al. Fabrication and temperature dependent magnetic properties of nickel nanowires embedded in alumina templates. Ceram. Int. 2015;41(9):12081–6.
[36] Manna S, Kim JW, Lubarda MV, Wingert J, Harder R, Spada F, et al. Characterization of strain and its effects on ferromagnetic nickel nanocubes. AIP Adv. 2017;7(12):125025.
[37] Kan JJ, Lubarda MV, Chan KT, Uhlir V, Scholl A, Lomakin V, et al. Periodic chiral magnetic domains in single-crystal nickel nanowires. Phys Rev Materials 2018;2:064406.
[38] Jyoko Y, Kashiwabara S, Hayashi Y, Schwarzacher W. Characterization of electrodeposited magnetic nanostructures. J. Magn. Magn. Mater. 1999;198–199:239.
[39] Wernsdrfer W, Thirion C, Demoncy N, Pascard H, Mailly D. Magnetisation reversal by uniform rotation (Stoner-Wohlfarth model) in FCC cobalt nanoparticles. J. Magn. Magn. Mater. 2002;242–245:132.
[40] Oyarzún S, Tamion A, Tournus F, Dupuis V, Hillenkamp M. Size effects in the magnetic anisotropy of embedded cobalt nanoparticles: from shape to surface. Sci. Rep. 2015;5:14749.
[41] Burn DM, Atkinson D. Effective pinning energy landscape perturbations for propagating magnetic domain walls. Sci. Rep. 2016;6:34517.
[42] Proenca MP, Sousa CT, Escrig J, Ventura J, Vázquez M, Araujo JP. Magnetic interactions and reversal mechanisms in Co nanowire and nanotube arrays. J. Appl. Phys. 2013;113:093907.
[43] Hertel R. Computational micromagnetism of magnetization processes in nickel nanowires. J. Magn. Magn. Mater. 2022;249:251.